

Chiral symmetry analysis and rigid rotational invariance for the lattice dynamics of single-wall carbon nanotubes

Jin-Wu Jiang,¹ Hui Tang,¹ Bing-Shen Wang,² and Zhao-Bin Su^{1,3}

¹*Institute of Theoretical Physics, Chinese Academy of Sciences, Beijing 100080, China*

²*National Laboratory of Semiconductor Superlattice and Microstructure
and Institute of Semiconductor, Chinese Academy of Sciences, Beijing 100083, China*

³*Center for Advanced Study, Tsinghua University, Beijing 100084, China*

In this paper, we provide a detailed expression of the vibrational potential for the lattice dynamics of the single-wall carbon nanotubes (SWCNT) satisfying the requirements of the exact rigid translational as well as rotational symmetries, which is a nontrivial generalization of the valence force model for the planar graphene sheet. With the model, the low frequency behavior of the dispersion of the acoustic modes as well as the flexure mode can be precisely calculated. Based upon a comprehensive chiral symmetry analysis, the calculated mode frequencies (including all the Raman and infrared active modes), velocities of acoustic modes and the polarization vectors are systematically fitted in terms of the chiral angle and radius, where the restrictions of various symmetry operations of the SWCNT are fulfilled.

PACS numbers: 81.07.De, 63.22.+m

I. INTRODUCTION

Since the discovery¹ of carbon nanotubes, it stimulated extensive studies on the lattice dynamics of the single-wall carbon nanotubes (SWCNT).^{2,3,4,5,6} The SWCNT can be viewed as rolling up a two-dimensional graphitic lattice into a seamless cylinder.⁷ Among various studies, the zone-folding method was firstly applied to study the lattice dynamics of the SWCNT, which is migrated from that for the planar graphite sheet. It successfully accounts the general features of the phonon spectrum in SWCNT. However, unlike the electronic problems, on which this method is workable except for very narrow SWCNT, the results for the lattice vibration by the zone-folding were not very satisfactory,² particularly, it can not provide correct numbers of Raman and infrared (IR) modes of SWCNT.⁸

In recent a few years, the theoretical investigation on lattice dynamics of SWCNT has achieved many successful and interesting results. Using the rotational and helical symmetries, Popov *et al.*^{9,10} decomposed for the first time the lattice dynamics equation of the SWCNT into a six-dimensional eigenvalue problem. Analytical expression for the velocities of the acoustic modes are derived using Born's perturbation technique.¹¹ The translational and rotational sum rules expressed in terms of the force constant matrix¹¹ of the helical tube are also addressed in Ref. 10. Damnjanovic *et al.* applied the line group analysis to the lattice dynamics of SWCNT,^{12,13} and also obtained the generalized Bloch form by modified group projectors technique.^{14,15,16} They also calculated the phonon spectra in SWCNT with a modified force constant model^{17,18,19} in which certain kinematic constraints were imposed to achieve the twisting mode. The authors tried also to fit their calculated frequencies of the Raman and IR modes as functions of tube radius and chiral angle. In a series of papers Mahan and his collaborators^{20,21} worked on the lattice dynamics of the

SWCNT with various vibrational energy terms such as spring energy, in-plane or out-of-plane bond bending potential energies successively, and calculated the phonon spectrum for the achiral as well as chiral²² tubes. They realized that, to keep the twisting mode to be a zero mode in the long wave length limit, all the pieces of vibration energies under their consideration violating the global rotational invariance around axial axis should be ignored. The authors also interpreted the existence condition of the flexure mode, which is an inherent character for rods and plates. This mode also shows up in Popov *et al.*'s calculation but is absent in Damnjanovic *et al.*'s results.

However, as pointed out in Ref. 21, the commonly used expression for bond bending potential, even in addition with the kinematic constraints as in Refs 17 and 18, does not satisfy the rotational invariance condition, where the missing of the flexure mode is a kind of evidence. At the same time, the discussion on the rotational symmetry requirements to the potential terms in connection with the flexure mode is restricted only to those around the tube axis. The force model¹⁰ taken from that for the graphite²³ obeys the translational and rotational sum rules of the planar sheet but does not meet precisely the symmetry requirements of cylindrical warped hexagonal lattice sheet.

Actually, the rotational invariance symmetry, i.e., the potential energy must keep unchanged when a system is rigidly rotated, should play a nontrivial role for rod-like cylindrical lattice sheet. On the other hand, the intrinsic symmetry of the tube lattice structure would also lead to specific restriction on dynamic matrix. For a complete account of the symmetries of the lattice dynamics for the SWCNT, both aspects should be considered in a consistent way. This constitutes the basic scope of this paper.

As a continuation of the previously mentioned series of works, in this paper, we show the vibration potential,

i.e. force model, up in a detailed expression with the rigid translational and rotational invariance being precisely guaranteed, in which the curvature effect on bond lengths and bond angles is carefully considered. As its direct consequences, the flexure mode as well as the acoustic torsion mode can be correctly treated. Moreover we calculate the phonon spectrum with the proposed force model and carry out a full chiral symmetry analysis. Instead of previous case-to-case empirical forms,¹⁸ the frequencies of all Raman and IR active modes, the polarization characteristics of the modes, as well as the velocities of all four acoustic modes can be systematically fitted in terms of tube radius and chiral angle with the symmetry considerations.

As expected, our calculated results show that the curvature effect on bond lengths and bond angles would be no more negligible only for nanotubes of smaller radius. Meanwhile the nontrivial contribution for the θ dependence of various physical quantities is also effective only for tubes with enough small radius. For thin tubes with the diameter range such as $4 \sim 10$ Å, the warped graphene sheet model, on which our discussions are based, should be fairly applicable to the SWCNT. For tubes with diameter smaller than 4 Å approximately, the warped graphene sheet model might have to be improved by further optimizing its equilibrium lattice configuration,^{24,25,26,27} and the part of chiral symmetry analysis in this paper were not be valid any more. Such estimation is entirely consistent with the existing literatures.¹⁸

The present paper is organized as following. In Sec. II, after a brief description on notations, we present the detailed expression of the vibrational potential. The rigid rotational invariance and the comparisons with previous works are discussed. Subsection III A is devoted to a generic chiral symmetry analysis for various physical quantities, while the main results and relevant discussions on phonon spectrum calculations are presented in Subsec. III B. The paper ends with a brief summary in Sec. IV.

II. MODEL

A. Notations

The z axis in this paper is set along the tube axis and the x axis comes across the middle point of a C-C bond in Fig. 1. It is understood in this subsection that notations for cylindrically warped tubes are often introduced with the aid of those defined on the planar sheet.

As is well known, SWCNT can be notated by a chiral vector $\vec{R} = n_1\vec{a}_1 + n_2\vec{a}_2$ or equivalently, the radius r and chiral angle θ . Where \vec{a}_1 and \vec{a}_2 being the primitive lattice vectors in graphite lattices,² $|\vec{a}_1| = |\vec{a}_2| = 2.46$ Å.

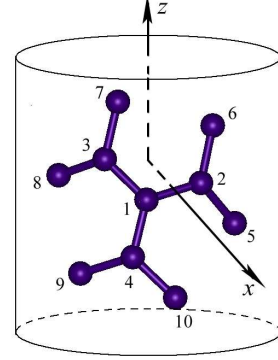


FIG. 1: The sketch of carbon atoms on a cylindric surface.

They have the relations as

$$r = \frac{|\vec{a}_1|}{2\pi} \sqrt{n_1^2 + n_1n_2 + n_2^2}, \quad \theta = \text{atan} \frac{\sqrt{3}n_2}{2n_1 + n_2}. \quad (1)$$

We use the helical and rotational symmetry descriptions for the SWCNT throughout this paper. Introduce a real lattice vector $\vec{H} = p_1\vec{a}_1 + p_2\vec{a}_2$ describing the screw operation⁷ with $n_1p_2 - n_2p_1 = N$ (N is the greatest common divisor of n_1 and n_2). The rotational angle of the screw operation is $\alpha = (\vec{H} \cdot \vec{R})/|\vec{R}|^2$ (in the unit of 2π). A unit cell in the (n_1, n_2) tubule can be notated by two equivalent ways, either based on $(\vec{H}, \frac{\vec{R}}{N})$, or on (\vec{a}_1, \vec{a}_2) as

$$\vec{r}_{m,l} = m\vec{H} + l\frac{\vec{R}}{N}, \quad \text{or} \quad \vec{r}_{q_1,q_2} = q_1\vec{a}_1 + q_2\vec{a}_2 \quad (2)$$

with the relations

$$m = (n_1q_2 - n_2q_1)/N, \quad l = q_1p_2 - q_2p_1. \quad (3)$$

In the following, we use $(\vec{H}, \frac{\vec{R}}{N})$ as the basic vectors, and \vec{b}_H and \vec{b}_R are their corresponding reciprocal unit vectors. Any wave vector in the reciprocal space can be written as

$$\vec{K} = \frac{\kappa}{2\pi} \vec{b}_H + \frac{n}{N} \vec{b}_R. \quad (4)$$

In the first Brillouin zone, $\kappa \in (-\frac{1}{2}, \frac{1}{2}]$ and n is an integer in $(-\frac{N}{2}, \frac{N}{2}]$.

B. Potentials

It had been proposed²³ that there are five distinctive terms for the vibrational potential of the graphene sheet satisfying the rigid translational and rotational invariance of the planar sheet. We herein present a detailed expression of the vibrational potential for the SWCNT with

the curvature effect being carefully in-cooperated, which is essentially the generalization of that for the graphene sheet. It satisfies precisely the requirements of the rigid translational and rotational invariance and realizes the corresponding general symmetry sum rules in Ref. 10, i.e., the potential energy must keep vanish term by term when the tube is rigidly translated or rotated around any axis. Introduce \vec{r}_i as the equilibrium position of atom i and \vec{u}_i as its displacement vector. $\vec{r}_{ij} = \vec{r}_j - \vec{r}_i$ is the vector from atom i to j in the nanotube while the modulus r_{ij} represents the length of C-C bond between atoms i and j . \vec{r}_i is determined following the geometry of a warped graphene sheet so that the three tridental bonds nearest-neighbored with the atom i as well as the angles between any of the two bonds are not equal to each other, especially for thin tubes.

The five potential terms for the SWCNT are expressed in the following.

(1) V_l is the potential of the spring force between the nearest-neighbor atom pair,

$$V_l = \frac{k_l}{2} \sum_{i=2}^4 [(\vec{u}_i - \vec{u}_1) \cdot \vec{e}_{1i}^l]^2, \quad (5)$$

where k_l is the first-order force constant and $\vec{e}_{1i}^l = \frac{\vec{r}_{1i}}{|\vec{r}_{1i}|}$. We'd like to point out that the components of the displacement vectors perpendicular to \vec{e}_{1i}^l which violates the rigid rotational invariance are forbidden.

(2) V_{sl} is also the potential of the spring force but between the next nearest-neighbored atoms illustrated as (1, 5 ... 10) in Fig. 1,

$$V_{sl} = \frac{k_{sl}}{2} \sum_{i=5}^{10} [(\vec{u}_i - \vec{u}_1) \cdot \vec{e}_{1i}^s]^2 \quad (6)$$

with k_{sl} the second-order force constant.

(3) The potential energy for the in-surface bond bending V_{BB} is actually a term associated with bond angle variations. Three atoms have to be considered together, and

$$\begin{aligned} V_{BB} &= \frac{k_{BB}}{4} \sum_{j_i} \sum_{\substack{j'_i \\ (j'_i \neq j_i)}} \left[\frac{\vec{u}_{j_i} - \vec{u}_i}{r_{ij_i}} \cdot (\vec{e}_{ij'_i}^l - \cos \theta_{j_i j'_i} \vec{e}_{ij_i}^l) \right. \\ &\quad \left. + \frac{\vec{u}_{j'_i} - \vec{u}_i}{r_{ij'_i}} \cdot (\vec{e}_{ij_i}^l - \cos \theta_{j'_i j_i} \vec{e}_{ij'_i}^l) \right]^2 \\ &= \frac{k_{BB}}{4} \sum_{j_i} \sum_{\substack{j'_i \\ (j'_i \neq j_i)}} (\cos \theta'_{j_i j'_i} - \cos \theta_{j_i j'_i})^2. \end{aligned} \quad (7)$$

If i is 1 or 2, j_i, j'_i take the sites 2, 3, 4 or 1, 5, 6 respectively. In Eq. (7), $\theta_{j_i j'_i}$ stands for the equilibrium angle between the bonds \vec{r}_{ij_i} and $\vec{r}_{ij'_i}$, while $\theta'_{j_i j'_i}$ for the corresponding angle in vibration. The expression in terms of $\vec{u}_{j_i} - \vec{u}_i$ and $\vec{u}_{j'_i} - \vec{u}_i$ is an honest representation to that of $\cos \theta'$, where the rigid rotational invariance referred

to an arbitrary axis can be kept only when the differences among bond lengths and bond angles be carefully accounted.

(4) The potential of the out-of-surface bond bending V_{rc} is the energy between atom i and the three nearest-neighbor atoms j_i with four atoms simultaneously contained,

$$V_{rc} = \frac{k_{rc}}{2} [(3\vec{u}_i - \sum_{j_i} \vec{u}_{j_i}) \cdot \vec{e}_i^{rc}]^2, \quad (8)$$

$$\vec{e}_i^{rc} = - \frac{\sum_{j_i} \vec{r}_{j_i}}{|\sum_{j_i} \vec{r}_{j_i}|}, \quad (9)$$

Where i takes 1 or 2 with j_i running over the three nearest neighbors of atom i . This potential has the physical intuition as that responsible for the radial optical mode in tubes and is trying to keep the four atoms on the cylinder surface. Herein we introduce an unit vector \vec{e}_i^{rc} defined in Eq. (9), which is rather close but not equal to the radial unit vector of site 1 shown in Fig. 2. When the radius is large enough, the \vec{e}_i^{rc} would be close enough to the \vec{e}_1^r . However, we stress that the potential term V_{rc} with \vec{e}_i^{rc} keeps the rigid rotational invariance while that with \vec{e}_i^r substituted by \vec{e}_i^r would break the rotational symmetry.

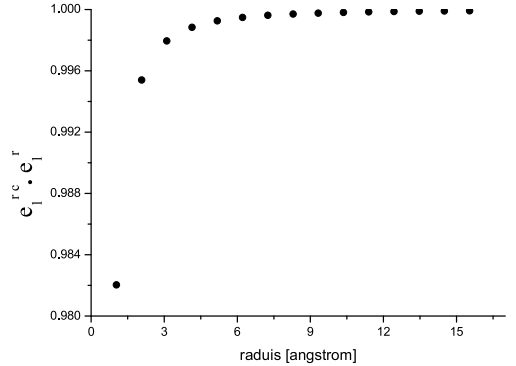


FIG. 2: The projection of \vec{e}_1^{rc} on \vec{e}_1^r for tubes $(2n, n)$ with $n \in [1, 15]$. It shows that \vec{e}_1^{rc} only deviates about 2% from \vec{e}_1^r even in the small radius (2, 1) tube.

(5) The twist potential energy for bond \vec{r}_{1k} is

$$V_{tw} = \frac{k_{tw}}{2} \sum_{\langle i, j \rangle} [(\vec{u}_i - \vec{u}_j - (\vec{u}_{i'} - \vec{u}_{j'})) \cdot \vec{e}_{1k}^r]^2, \quad (10)$$

where \vec{e}_{1k}^r is the unit vector along the radial direction of the middle point of \vec{r}_{1k} , $\langle i, j \rangle$ represents a pair of atoms nearest-neighbored with atom 1 while k the third of its nearest neighbors. Pair $\langle i', j' \rangle$ is the image of $\langle i, j \rangle$ referring to a C_2 rotation around the axis in \vec{e}_{1k}^r . It has the intuition that responsible for modes with twisted vibrations.

C. Some details about the model

Obviously, all the five potential energy terms respect the translational invariance. When $\vec{u}_i = \vec{u}_j$, $\vec{u}_i - \vec{u}_j = 0$ leads to

$$V_l = V_{sl} = V_{BB} = V_{rc} = V_{tw} = 0.$$

For the rotational invariance, we have to consider the five potentials term by term separately.^{11,28} When the tube rotates rigidly around an arbitrary axis for a small angle $\delta\vec{\omega}$ with its direction along the axis $\frac{\delta\vec{\omega}}{|\delta\vec{\omega}|}$ and its magnitude $|\delta\vec{\omega}|$ being the totation angle, each lattice site acquires a displacement $\vec{u}_i = \delta\vec{\omega} \times \vec{r}_i$,

$$\vec{u}_i - \vec{u}_j = \delta\vec{\omega} \times (\vec{r}_i - \vec{r}_j) = \delta\vec{\omega} \times \vec{r}_{ji}. \quad (11)$$

Substituting Eq. (11) into the first two potential terms (5) and (6), it is straightforward to have $(\vec{u}_j - \vec{u}_i) \cdot \vec{e}_{ij}^t = r_{ij}(\delta\vec{\omega} \times \vec{e}_{ij}^t) \cdot \vec{e}_{ij}^t = 0$. Then

$$V_l = V_{sl} = 0.$$

Substituting Eq. (11) into the third potential term (7), a typical representative term in summation becomes

$$V_{BB} \sim \frac{k_{BB}}{4} [\delta\vec{\omega} \cdot (\vec{e}_{12}^t \times \vec{e}_{13}^t + \vec{e}_{13}^t \times \vec{e}_{12}^t)]^2 = 0.$$

In which a fact has been used that r_{ij} in the denominate is cancelled by that in the numerator when Eq. (11) is applied. Moreover, for each typical representative term in potentials (8) and (10), we have similarly,

$$V_{rc} \sim \frac{k_{rc}}{2} [\delta\vec{\omega} \times (\vec{r}_{12} + \vec{r}_{13} + \vec{r}_{14}) \cdot \vec{e}_1^c]^2 = 0, \\ V_{tw} \sim \frac{k_{tw}}{2} [\delta\vec{\omega} \times (\vec{r}_{43} - \vec{r}_{56}) \cdot \vec{e}_{12}^t]^2 = 0.$$

As an example for further clarification, one might calculate the phonon spectrum with all the bond lengths and bond angles assumed to be equal to that of the graphite. It results that the twisting mode (TW) at $(\kappa, n) = (0, 0)$ is no longer a zero mode and there is a finite gap. For the SWCNT (5,2), the error introduced by the equal-bond-length creates a gap of the order 0.5 cm^{-1} as shown in Fig. 3, where the radius $r = 2.45 \text{ \AA}$, the three C-C bonds are about -1.3% , -0.3% and 0.0% shorter than that of graphite 1.42 \AA respectively. Although it is a minute number and entirely negligible in practice, it is of qualitative significance.

As a distinguished feature of the nanotubes that the two degenerate transversal acoustic (TA) modes shown up at $(\kappa, n) = \pm(\alpha, 1)$ are flexure modes. Instead of the conventional linear behaviors, the low frequency limits of their dispersions are parabolic as $\omega^2 = \beta^2(\kappa \mp \alpha)^4$. We address that the rigid rotational invariance around z axis itself is not a sufficient condition for the existence of the flexure modes cf. Ref. 21. As a counter example, we introduce a term $V_{\tau i} = \frac{k_{\tau i}}{2} [(\vec{u}_2 - \vec{u}_1) \cdot \vec{e}_{12}^t]^2$ with $\vec{e}_{12}^t = \vec{e}_{12} \times \vec{e}_{12}^t$, which is the elastic energy due to the tangential spring force between atoms 1 and 2. It is easy

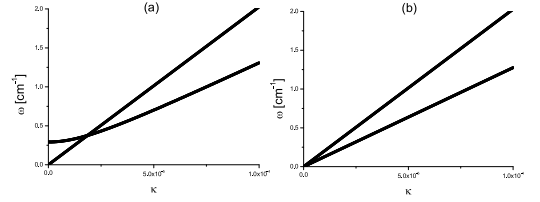


FIG. 3: The effect of bond lengths on TW mode in tube (5, 2). (a) All bonds are assumed to be the same. The frequency of TW mode is nonzero. (b) The differences between bonds are considered. The frequency of TW mode is precisely zero.

to verify that $V_{\tau i} = 0$ when the tube rotates around the z axis. But there is no flexure mode when $V_{\tau i}$ is taken into account.¹⁸ This is because that $V_{\tau i}$ would be no more zero when the tube rotates around any axis perpendicular to the z axis.

III. RESULTS AND DISCUSSIONS

A. Further symmetry considerations

We may establish a mapping from the space of chiral vectors on the planar sheet to that of the nanotube structure in a fixed way of wrapping²⁹

$$f : \{\text{chiral vector set}\} \mapsto \{\text{nanotube set}\}.$$

However this is not a one-to-one mapping. As mentioned in Ref. 29, a given SWCNT can be equivalently composed by three chiral vectors \vec{R}_0 , \vec{R}_2 and \vec{R}_4 with chiral angles as θ , $\theta + 2\pi/3$ and $\theta + 4\pi/3$ respectively within the corresponding graphite sheet. Due to the \hat{C}_{6v} symmetry of the hexagonal graphene lattice sheet, there is another set of vectors \vec{R}_1 , \vec{R}_3 and \vec{R}_5 with chiral angles as $\theta + \pi/3$, $\theta + \pi$ and $\theta + 5\pi/3$ respectively on the graphite sheet. These three chiral vectors correspond again to the same SWCNT which is actually the nanotube by rotating the tube formed by \vec{R}_0 upside down, i.e. a \hat{C}_{2x} operation. The net result of the operation is an exchange of A and B carbon atoms in unit cells with the sign of its chiral index $\nu = \text{mod}\{n_1 - n_2, 3\}$ also changed. There is one another operation $\hat{\sigma}_{xz}$ connecting a pair of SWCNT which is the mirror reflection onto each other with respect to xz plane. Correspondingly \vec{R}_0 in the sheet is changed into its counterpart \vec{R}'_0 with $\theta \rightarrow -\theta$ but ν kept unchanged.

As one of the direct consequences of the above observations, any physical quantity $Q^\nu(r, \theta)$ of the SWCNT is a periodical function of the chiral angle θ with period $\frac{2\pi}{3}$, i.e., $Q^\nu(r, \theta)$ can be expanded as²⁹

$$Q^\nu(r, \theta) = \sum_{n=0}^{\infty} a_n^\nu \cos(3n\theta) + b_n^\nu \sin(3n\theta). \quad (12)$$

Furthermore, under the operation $\theta \rightarrow \theta + \pi/3$, any scalars S would keep unchanged. For normal vectors, the

radial components have the same behavior, but the azimuthal and axial components change signs²⁹. That is

$$\begin{cases} S^\nu(\theta + \frac{\pi}{3}) = S^{-\nu}(\theta), \\ \vec{v}^\nu(\theta + \frac{\pi}{3}) = \hat{C}_{2x}\vec{v}^{-\nu}(\theta) \end{cases} \quad (13)$$

with $\hat{C}_{2x}\vec{e}_r = \vec{e}_r$, $\hat{C}_{2x}\vec{e}_\phi = -\vec{e}_\phi$, $\hat{C}_{2x}\vec{e}_z = -\vec{e}_z$. Here \vec{e}_r , \vec{e}_ϕ and \vec{e}_z are unit vectors oriented towards radial, azimuthal and axial directions upon the cylindrical surface respectively.

In addition, operation $\hat{\sigma}_{xz}$ gives that any scalars or radial and axial components of vectors are even functions of θ , while azimuthal components are odd functions of θ ,²⁹

$$\begin{cases} S^\nu(-\theta) = S^\nu(\theta), \\ \vec{v}^\nu(-\theta) = \hat{\sigma}_{xz}\vec{v}^\nu(\theta) \end{cases} \quad (14)$$

with $\hat{\sigma}_{xz}\vec{e}_r = \vec{e}_r$, $\hat{\sigma}_{xz}\vec{e}_\phi = -\vec{e}_\phi$, $\hat{\sigma}_{xz}\vec{e}_z = \vec{e}_z$. The detailed expressions reduced from Eq. (12) due to the symmetry restrictions Eqs (13) and (14) are shown in the appendix.

B. Frequencies, acoustic velocities, and eigenvectors

We calculated the phonon spectrum in the (κ, n) representation with the vibrational potential Eqs (5)-(10). By tuning the calculated results to the experimental data³⁰ for the Raman modes of (10, 10) tube (see Table I), we fit the corresponding force constants as $k_l = 364.0 \text{ Nm}^{-1}$, $k_{sl} = 62.0 \text{ Nm}^{-1}$, $k_{BB} = 1.07 \times 10^{-11} \text{ erg}$, $k_{rc} = 14.8 \text{ Nm}^{-1}$, and $k_{tw} = 6.24 \text{ Nm}^{-1}$. We successfully identified 4 zero modes, 14 Raman active modes and 6 IR active modes for the chiral SWCNT.⁸ Two of the six modes at $(\kappa, n) = (0, 0)$ are zero modes. They are longitudinal acoustic (LA) and TW modes both belonging to ${}_0A_0^-$ representation (Reps). Another mode belonging also to ${}_0A_0^-$ Reps is the IR active \vec{e}_r optical (OP) mode with A and B atoms oscillating out of surface in radial direction. The other three nonzero modes at $(\kappa, n) = (0, 0)$ belonging to ${}_0A_0^+$ Reps are Raman active, they are \vec{e}_r acoustic (AC), \vec{e}_θ OP and \vec{e}_z OP. There are one flexure and five nonzero modes at $(\kappa, n) = (\alpha, 1)$. The latter are both Raman and IR active assigned to ${}_\alpha E_1$ Reps. At $(\kappa, n) = (2\alpha, 2)$, six nonzero modes are all Raman active belonging to the same ${}_{2\alpha} E_2$ Reps.

We also calculated the sound velocities of LA and TW modes, the flexure parabolic coefficient for the TA mode, and polarizations of nonzero modes at $(\kappa, n) = (0, 0)$ for varieties of tubes as the functions of r and θ . The modes at $(\kappa, n) = (\alpha, 1)$ as well as $(2\alpha, 2)$ are doubly degenerated with their one-to-one degenerate counterparts at $(-\alpha, -1)$ and $(-2\alpha, -2)$ respectively. In Fig. 4, we provide the three-dimensional plots for some of these quantities as functions of r and θ .

Our calculated results are further fitted following the parameterization shown in Eq. (12). The corresponding expressions for the frequencies of above 15 Raman and IR active modes, the velocities and flexure

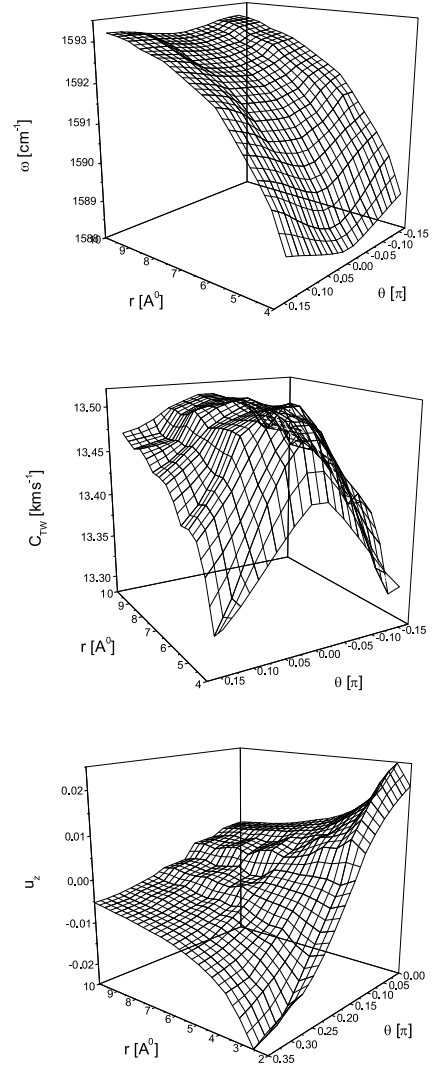


FIG. 4: As functions of r and θ , we show in (a) the frequency of \vec{e}_r OP mode at $(\kappa, n) = (0, 0)$; (b) C_{TW} for small radius tubes; (c) the z component of the eigenvector of \vec{e}_r AC mode.

parabolic, and the polarization vectors of nonzero modes at $(\kappa, n) = (0, 0)$ are listed in Tables II, III, and IV respectively. In this paper particular emphasis is drawn to tubes with smaller radius. So we take the parameter regime for frequencies and velocities in $r \in [4.0, 10.0] \text{ Å}$ and $\theta \in [-\frac{\pi}{6}, \frac{\pi}{6}]$, while that for polarization vectors in $r \in [2.0, 10.0] \text{ Å}$ and $\theta \in [-\frac{\pi}{3}, \frac{\pi}{3}]$. We keep the relative errors in fitting less than 5×10^{-4} . The above parameter regimes are such chosen only for tubes of smaller radius, in which the contributions of θ dependence are notable comparing to those of r dependence. The velocity of the TW mode (in Table III) as well as the polarization vectors of modes with ${}_0A_0^+$ Reps (in Table IV) are typical examples shown up an evident θ dependence. In fact, the corresponding calculations have also been carried out in the parameter regime $r \in [3.13, 58.7] \text{ Å}$. The results

TABLE I: Comparison between the calculated results (following our model) and the experimental values for several mode frequencies (in the unit of cm^{-1}) of SWCNT (10,10).

Reps	${}_0A_0^+$	${}_0A_0^+$	${}_0E_1^-$	${}_0E_1^-$	$2{}_0E_2^+$	$2{}_0E_2^+$	$2{}_0E_2^+$	$2{}_0E_2^+$
theory	167	1588	105	1588	21	367	873	1584
experiment ³⁰	186	1593	118	1567	/	377	/	1606

TABLE II: Frequencies (in the unit of cm^{-1}) of 15 Raman and IR active modes as functions of r (in Å) and θ .

Reps	Mode/Order	$\omega(\theta)$	$f_i(r)$
${}_0A_0^+$ R	\vec{e}_r AC, 1	$f_0(r)$	$f_0(r) = \frac{1133.86}{r} - \frac{139.65}{r^3}$
	\vec{e}_θ OP, 2	$f_0(r) + f_1(r) \cos 6\theta$	$f_0(r) = 1594.00 - \frac{266.98}{r^2}, f_1(r) = \frac{8.65}{r^2}$
	\vec{e}_z OP, 3	$f_0(r) + f_1(r) \cos 6\theta + f_2(r) \cos 12\theta$	$f_0(r) = 1594.00 - \frac{91.81}{r^2}, f_1(r) = -\frac{15.68}{r^2}, f_2(r) = -\frac{0.68}{r^2}$
${}_0A_0^-$ Ir	\vec{e}_r OP, 4	$f_0(r) + f_1(r) \cos 6\theta$	$f_0(r) = 864.81 + \frac{990.22}{r^2} - \frac{1117.30}{r^4}, f_1(r) = \frac{9.16}{r^2}$
${}_0E_1$ R Ir	1	$f_0(r) + f_1(r) \cos 6\theta$	$f_0(r) = \frac{710.16}{r} + \frac{45.07}{r^3}, f_1(r) = \frac{1.99}{r^3} - \frac{31.55}{r^4}$
	2	$f_0(r) + f_1(r) \cos 6\theta$	$f_0(r) = \frac{1603.51}{r} - \frac{746.51}{r^3}, f_1(r) = -\frac{115.54}{r^3}$
	3	$f_0(r) + f_1(r) \cos 6\theta$	$f_0(r) = 864.84 + \frac{860.00}{r^2} - \frac{1758.70}{r^4}, f_1(r) = \frac{11.63}{r^2} - \frac{206.52}{r^4}$
	$\nu = \pm 1, 4$	$f_0(r) \pm f_1(r) \cos 9\theta$	$f_0(r) = 1594.13 - \frac{316.67}{r^2}, f_1(r) = \frac{31.92}{r^3}$
	$\nu = 0, 4$	$f_0(r) + f_1(r) \cos 6\theta + f_2(r) \cos 12\theta$	$f_0(r) = 1594.14 - \frac{318.48}{r^2}, f_1(r) = \frac{7.83}{r^2} - \frac{19.03}{r^4}$ $f_2(r) = \frac{2.70}{r^2} + \frac{0.60}{r^4}$
	5	$f_0(r) + f_1(r) \cos 6\theta$	$f_0(r) = 1593.97 - \frac{277.49}{r^2}, f_1(r) = -\frac{12.45}{r^2}$
$2{}_0E_2$ R	1	$f_0(r) + f_1(r) \cos 6\theta + f_2(r) \cos 12\theta$	$f_0(r) = \frac{959.33}{r^2} - \frac{736.60}{r^4} + \frac{779.59}{r^6}$ $f_1(r) = \frac{6.19}{r^3} + \frac{73.37}{r^4}, f_2(r) = -\frac{0.06}{r^3} + \frac{9.34}{r^4}$
	2	$f_0(r) + f_1(r) \cos 6\theta$	$f_0(r) = \frac{1420.21}{r} + \frac{54.52}{r^3} - \frac{1246.29}{r^5}, f_1(r) = \frac{204.34}{r^3}$
	3	$f_0(r) + f_1(r) \cos 6\theta$	$f_0(r) = \frac{2535.48}{r} - \frac{2426.65}{r^3}, f_1(r) = -\frac{412.23}{r^3}$
	4	$f_0(r) + f_1(r) \cos 6\theta$	$f_0(r) = 864.80 + \frac{486.71}{r^2} - \frac{4711.81}{r^4} + \frac{12425.61}{r^6}$ $f_1(r) = \frac{9.89}{r^2} - \frac{524.74}{r^4}$
	5	$f_0(r) + f_1(r) \cos 6\theta$	$f_0(r) = 1594.00 - \frac{869.19}{r^2} + \frac{978.77}{r^4}$ $f_1(r) = -\frac{16.15}{r^2} + \frac{363.41}{r^4}$
	6	$f_0(r) + f_1(r) \cos 6\theta$	$f_0(r) = 1594.01 - \frac{392.92}{r^2} - \frac{2160.15}{r^4} + \frac{5416.26}{r^6}$ $f_1(r) = \frac{7.88}{r^2} - \frac{297.88}{r^4}$

can be fitted very well by the same functions with minor change of coefficients, i.e., our fitting formulae could be applied to a much wider parameter regime.

It is interesting to see that all the numerically fitting expressions meet the symmetry requirements of Eqs (13) and (14), where the velocities and frequencies are of scalars while polarizations are of vectors. We notice that in Table II, one of the ${}_0E_1$ modes manifests different parameter dependence for different chiral index ν , i.e. it has different expressions for $\nu = \pm 1$ and $\nu = 0$ respectively. However, it is still consistent with the general expressions Eqs (13) and (14). We further notice that, different from those physical quantities of normal vectors, the polarization vector can be measured up to a global phase factor as ± 1 . Therefore, the corresponding trans-

formation properties with respect to $\theta \rightarrow \theta + \frac{\pi}{3}$ as well as $\theta \rightarrow -\theta$ need to be generalized to

$$\begin{cases} v_P^{\nu(m)}(\theta + \frac{\pi}{3}) = \lambda^{(m)}(\hat{C}_{2x}) \hat{C}_{2x} v_P^{\nu(m)}(\theta), \\ v_P^{\nu(m)}(-\theta) = \lambda^{(m)}(\hat{\sigma}_{xz}) \hat{\sigma}_{xz} v_P^{\nu(m)}(\theta), \end{cases} \quad (15)$$

respectively, in which $\lambda^{(m)}(\hat{o})$ is the phase factor taking value 1 or -1 corresponding to mode m such as \vec{e}_r AC, \vec{e}_ϕ OP and \vec{e}_z OP and referring to the symmetry operation \hat{o} such as \hat{C}_{2x} and $\hat{\sigma}_{xz}$. In particular, we have

$$\begin{aligned} \lambda^{(\vec{e}_r \text{ AC})}(\hat{C}_{2x}) &= \lambda^{(\vec{e}_r \text{ AC})}(\hat{\sigma}_{xz}) = 1, \\ \lambda^{(\vec{e}_\phi \text{ OP})}(\hat{C}_{2x}) &= \lambda^{(\vec{e}_\phi \text{ OP})}(\hat{\sigma}_{xz}) = -1, \\ \lambda^{(\vec{e}_z \text{ OP})}(\hat{C}_{2x}) &= -\lambda^{(\vec{e}_z \text{ OP})}(\hat{\sigma}_{xz}) = -1. \end{aligned}$$

TABLE III: Sound velocities (in kms^{-1}) of the TW and LA modes, and β (in $10^{-6}\text{m}^2\text{s}^{-1}$) of the flexure mode as functions of r (in \AA) and θ .

Velocity	Velocity(θ)	$f_i(r)$
C_{TW}	$f_0(r) + f_1(r) \cos 6\theta$	$f_0 = 13.5 - \frac{1.63}{r^2}, f_1 = \frac{2.38}{r^2}$
C_{LA}	$f_0(r) + f_1(r) \cos 6\theta$	$f_0 = 21.0706 + \frac{0.0055}{r} - \frac{0.6860}{r^2}, f_1 = \frac{0.00091}{r} - \frac{0.01679}{r^2}$
β	$f_0(r) + f_1(r) \cos 6\theta$	$f_0 = 1.3767r - 0.00142r^2 - 5.8 \times 10^{-5}r^3, f_1 = -\frac{0.143}{r} + \frac{0.04994}{r^3}$

TABLE IV: Polarization vectors $\vec{u} \equiv (\vec{u}(A), \vec{u}(B))$ as functions of r (in \AA) and θ . Where $\vec{u}(A)$ and $\vec{u}(B)$ indicate the displacement vectors of atoms A and B in the $(0, 0)$ unit cell respectively. For the three modes in this table, $u_r(B) = u_r(A)$, $u_\phi(B) = -u_\phi(A)$, $u_z(B) = -u_z(A)$.

$(\kappa, n) = (0, 0)$		Vector(θ)	$f_i(r)$
R_1 (\vec{e}_r AC)	$u_r(A)$	$f_0(r)$	$f_0(r) = 0.7071 - \frac{0.0028}{r^2}$
	$u_\phi(A)$	$f_1(r) \sin 3\theta$	$f_1(r) = \frac{0.0518}{r} + \frac{0.0468}{r^2}$
	$u_z(A)$	$f_1(r) \cos 3\theta$	$f_1(r) = \frac{0.0517}{r} + \frac{0.0749}{r^2}$
R_2 (\vec{e}_ϕ OP)	$u_r(A)$	$f_1(r) \sin 3\theta$	$f_1(r) = -\frac{0.0542}{r} - \frac{0.0455}{r^2}$
	$u_\phi(A)$	$f_0(r) + f_1(r) \cos 12\theta$	$f_0(r) = 0.7056 + \frac{0.0019}{r^2}, f_1(r) = 0.0015 - \frac{0.003}{r^2}$
	$u_z(A)$	$f_1(r) \sin 6\theta + f_2(r) \sin 12\theta$	$f_1(r) = 0.0656 - \frac{0.0801}{r^2}, f_2(r) = 0.0048 - \frac{0.0112}{r^2}$
R_3 (\vec{e}_z OP)	$u_r(A)$	$f_1(r) \cos 3\theta$	$f_1(r) = -\frac{0.0447}{r} - \frac{0.0417}{r^2}$
	$u_\phi(A)$	$f_1(r) \sin 6\theta + f_2(r) \sin 12\theta$	$f_1(r) = -0.0656 + \frac{0.0773}{r^2}, f_2(r) = -0.0048 + \frac{0.0111}{r^2}$
	$u_z(A)$	$f_0(r) + f_1(r) \cos 12\theta$	$f_0(r) = 0.7056 + \frac{0.0019}{r^2}, f_1(r) = 0.0015 - \frac{0.0033}{r^2}$

It can be easily verified that the parameterized expressions for the modes \vec{e}_r AC, \vec{e}_ϕ OP and \vec{e}_z OP listed in Table IV satisfy exactly Eq. (15). Interestingly, the values taken by $\lambda^{(m)}(\hat{o})$ coincide precisely with the signatures of the major component of the corresponding modes with respect to the operations \hat{C}_{2x} and $\hat{\sigma}_{xz}$. The detailed expressions for polarization vectors are given in the appendix.

It is known that the planar graphene is the $r \rightarrow \infty$ limit of the SWCNT. We notice that six modes in Table II evolve to the two degenerate in-plane optical modes of the graphene with approximately the same frequency limit 1594.0. While three modes with $f_0(r) \rightarrow 864.8$ approach the out-of-plane optical mode of the graphene sheet. Moreover shown in Table III, the sound velocities of the two zero modes, i.e. LA and TW modes belonging to ${}_0A_0^-$, have nonzero limits with different values. Therefore, it is expected that those two modes would approach two acoustic modes of the graphene sheet. We further notice that the frequency of the \vec{e}_r AC mode belonging to ${}_0A_0^+$ (Table II) vanishes with its polarization vector perpendicular to the limiting sheet. We might interpret that this mode is a kind of precursor of the flexure mode of the graphitic sheet. However, at $(\kappa, n) = \pm(\alpha, 1)$, the dispersion of the TA branch is quadratic in κ . We stress that the parameterization for the coefficient β cannot be extrapolated to $r \rightarrow \infty$. This is prohibited by a kind of symmetry argument that the rod-like tube has two

flexure modes with the cylindrical symmetry while the plate-like graphene sheet breaks the symmetry so as to have only one flexure mode. There is no way to cross continuously from the former to the latter.

The sound velocities, slopes of the dispersions, of zero modes can be determined correctly only if we have enough data of the dispersions with high precision in the low frequency limit around $(\kappa, n) = (0, 0)$. As one of the immediate consequences of our calculations, besides that for C_{LA} , our calculations provide a credible value for C_{TW} by taking the advantage that our model keeps exactly the translational and rotational invariance. With the velocities C_{LA} and C_{TW} we can extract the chirality-dependent expression for the Poisson ratio μ .¹⁰ Ignoring $\frac{1}{r^4}$ and higher order terms, we get

$$\mu = 0.21 + \frac{0.206}{r^2} - \frac{0.43}{r^2} \cos 6\theta. \quad (16)$$

We may take the values of θ as either $\frac{\pi}{6}$ (armchair) or 0 (zigzag) in the above Eq. (16) to extract the Poisson ratios for the achiral cases:

$$\begin{aligned} \mu &= 0.21 + \frac{0.636}{r^2}, & \text{for } \theta = \frac{\pi}{6}; \\ \mu &= 0.21 - \frac{0.224}{r^2}, & \text{for } \theta = 0. \end{aligned}$$

The corresponding results reported in Ref. 10 derived by the perturbation approach can be fitted by our expression in good agreement.

IV. CONCLUSIONS

In conclusion, we presented a detailed expression for the vibrational potential of the SWCNT. On the one hand, they obey precisely the rigid rotational and translational symmetries, in which the bond length differences as well as those of bond angles are properly considered following the geometry of cylindrically warped graphene sheet. On the other hand, they exhibit the chiral symmetry inherited from the planar hexagonal lattice. With this model we calculated the phonon spectrum of the SWCNT and parameterized the physical quantities in terms of tube diameter and chiral angle to make the chiral symmetry to be explicit. Our calculated results are mainly illustrated and summarized in Fig. 4 and Tables II, III, and IV. The physics of relevant quantities such as flexure modes, some of the immediate consequences like Poisson ratio, and the symmetry properties of, for example, the polarization vectors are discussed. Our paper provides a comprehensive and systematic understanding for the lattice dynamics of the SWCNT, and forms a kind of sound basis for further improvements and developments.

APPENDIX A: THE EXPRESSION FOR PHYSICAL QUANTITY

With the symmetry restriction as Eqs (13) and (14), i.e. $\lambda^{(m)}(C_{2x}) = \lambda^{(m)}(\sigma_{xz}) = 1$ in Eq. (15), the general expression Eq. (12) would reduce to the following.

Since the frequency ω is a scalar, we have

$$\begin{aligned}\omega^\pm(\theta) &= a_0 \pm a_1 \cos(3\theta) + a_2 \cos(6\theta) \pm a_3 \cos(9\theta) + \dots \\ \omega^0(\theta) &= a_0 + a_2 \cos(6\theta) + \dots\end{aligned}\quad (A1)$$

The three components of a vector can be expanded as

$$\begin{aligned}v_r^\nu(\theta) &= \sum_{n=0}^{\infty} \nu^{[\frac{1+(-1)^n}{2}]} a_n \cos 3n\theta \\ &= a_0 + \nu a_1 \cos 3\theta + a_2 \cos 6\theta + \dots, \\ v_\phi^\nu(\theta) &= \sum_{n=0}^{\infty} \nu^{[\frac{1+(-1)^n}{2}]} b_n \sin 3n\theta \\ &= b_1 \sin 3\theta + \nu b_2 \sin 6\theta + \dots, \\ v_z^\nu(\theta) &= \sum_{n=0}^{\infty} \nu^{[\frac{1+(-1)^n}{2}]} a_n \cos 3n\theta\end{aligned}$$

$$= \nu a_0 + a_1 \cos 3\theta + \nu a_2 \cos 6\theta + \dots \quad (A2)$$

Moreover, for polarization vectors, when $\lambda^m(\sigma_{xz}) = -1$, and $\lambda^m(C_{2x}) = -1$, we have

$$\begin{aligned}v_r^\nu(\theta) &= \sum_{n=0}^{\infty} \nu^{[\frac{1+(-1)^n}{2}]} b_n \sin 3n\theta \\ &= b_1 \sin 3\theta + \nu b_2 \sin 6\theta + \dots, \\ v_\phi^\nu(\theta) &= \sum_{n=0}^{\infty} \nu^{[\frac{1+(-1)^n}{2}]} a_n \cos 3n\theta \\ &= a_0 + \nu a_1 \cos 3\theta + a_2 \cos 6\theta + \dots, \\ v_z^\nu(\theta) &= \sum_{n=0}^{\infty} \nu^{[\frac{1+(-1)^n}{2}]} b_n \sin 3n\theta \\ &= \nu b_1 \sin 3\theta + b_2 \sin 6\theta + \dots\end{aligned}\quad (A3)$$

When $\lambda^m(\sigma_{xz}) = 1$, and $\lambda^m(C_{2x}) = -1$, we have

$$\begin{aligned}v_r^\nu(\theta) &= \sum_{n=0}^{\infty} \nu^{[\frac{1+(-1)^n}{2}]} a_n \cos 3n\theta \\ &= \nu a_0 + a_1 \cos 3\theta + \nu a_2 \cos 6\theta + \dots, \\ v_\phi^\nu(\theta) &= \sum_{n=0}^{\infty} \nu^{[\frac{1+(-1)^n}{2}]} b_n \sin 3n\theta \\ &= \nu b_1 \sin 3\theta + b_2 \sin 6\theta + \dots, \\ v_z^\nu(\theta) &= \sum_{n=0}^{\infty} \nu^{[\frac{1+(-1)^n}{2}]} a_n \cos 3n\theta \\ &= a_0 + \nu a_1 \cos 3\theta + a_2 \cos 6\theta + \dots\end{aligned}\quad (A4)$$

When $\lambda^m(\sigma_{xz}) = -1$, and $\lambda^m(C_{2x}) = 1$, we have

$$\begin{aligned}v_r^\nu(\theta) &= \sum_{n=0}^{\infty} \nu^{[\frac{1+(-1)^n}{2}]} b_n \sin 3n\theta \\ &= \nu b_1 \sin 3\theta + b_2 \sin 6\theta + \dots, \\ v_\phi^\nu(\theta) &= \sum_{n=0}^{\infty} \nu^{[\frac{1+(-1)^n}{2}]} a_n \cos 3n\theta \\ &= \nu a_0 + a_1 \cos 3\theta + \nu a_2 \cos 6\theta + \dots, \\ v_z^\nu(\theta) &= \sum_{n=0}^{\infty} \nu^{[\frac{1+(-1)^n}{2}]} b_n \sin 3n\theta \\ &= b_1 \sin 3\theta + \nu b_2 \sin 6\theta + \dots\end{aligned}\quad (A5)$$

¹ S. Iijima, Nature(London) **354**, 56 (1991).

² R. Saito, G. Dresselhaus, and M.S. Dresselhaus, *Physical Properties of Carbon Nanotubes* (Imperial College Press, 1998).

³ R.A. Jishi, M.S. Dresselhaus, and G. Dresselhaus, Phys. Rev. B **48**, 11385 (1993).

⁴ R. Saito, T. Takeya, T. Kimura, G. Dresselhaus, and M.S. Dresselhaus, Phys. Rev. B **57**, 4145 (1998).

⁵ R.A. Jishi, L. Venkataraman, M.S. Dresselhaus, and G. Dresselhaus, Chem. Phys. Lett. **209**, 77 (1993).

⁶ M.S. Dresselhaus, and P.C. Eklund, Adv. Phys. **49**, 705 (2000).

⁷ C.T. White, D.H. Robertson, and J.W. Mintmire, Phys. Rev. B **47**, 5485 (1993).

⁸ Ofir E. Alon, Phys. Rev. B **63**, 201403 (2001).

⁹ V.N. Popov, V.E. Van Doren, and M. Balkanski, Phys.

- Rev. B **59**,8355 (1999).
- ¹⁰ V.N. Popov, V.E. Van Doren, and M. Balkanski, Phys. Rev. B **61**,3078(2000).
 - ¹¹ M. Born and K. Huang, *Dynamical Theory of Crystal Lattices* (Oxford University Press, Oxford, 1954).
 - ¹² M. Damnjanović, I. Milošević, T. Vuković, and R. Sredanović, Phys. Rev. B **60**, 2728 (1999).
 - ¹³ M. Damnjanović, T. Vuković, and I. Milošević, J. Phys. A **33**, 6561 (2000).
 - ¹⁴ I. Milošević, and M. Damnjanović, Phys. Rev. B **47**, 7805 (1993).
 - ¹⁵ M. Damnjanović, and I. Milošević, J. Phys. A **27**, 4859 (1994).
 - ¹⁶ M. Damnjanović, and I. Milošević, J. Phys. A **28**, 1669 (1995).
 - ¹⁷ J. Maultzsch, S. Reich, C. Thomsen, E. Dobardžić, I. Milošević, and M. Damnjanović, Solid State Commun. **121**, 471 (2002).
 - ¹⁸ E. Dobardžić, I. Milošević, B. Nikolić, T.Vuković, and M. Damnjanović, Phys. Rev. B **68**,045408 (2003).
 - ¹⁹ I. Milošević, E. Dobardžić, and M. Damnjanović, Phys. Rev. B **72**,085426 (2005).
 - ²⁰ L.M. Woods, and G.D. Mahan, Phys. Rev. B **61**, 10651 (2000).
 - ²¹ G.D. Mahan, and Gun Sang Jeon, Phys. Rev. B **70**, 075405 (2004).
 - ²² Weihua Mu, and Zhong-can Ou-Yang, arXiv:cond-mat/0512570.
 - ²³ T. Aizawa, R. Souda, S. Otani, Y. Ishizawa, and C. Oshima, Phys. Rev. B **42**, 11469 (1990); **43**, 12060(E) (1991).
 - ²⁴ Daniel Sánchez-Portal, Emilio Artacho, José M. Soler, Angel Rubio, and Pablo Ordejón, Phys. Rev. B **59**, 12678 (1999).
 - ²⁵ J. Kürti, G. Kresse, and H. Kuzmany, Phys. Rev. B **58**, R8869 (1998).
 - ²⁶ I. Cabria, J.W. Mintmire, and C.T. White, Phys. Rev. B **67**, 121406 (2003).
 - ²⁷ Lianxi Shen, and Jackie Li, Phys. Rev. B **71**, 165427 (2005).
 - ²⁸ O. Madelung, *Introduction to Solid-State Theory*, Chap.3 (Springer-Verlag Berlin, Heidelberg, 1978).
 - ²⁹ Fei Ye, Bing-Shen Wang, and Zhao-Bin Su, arXiv:cond-mat/0511484.
 - ³⁰ A.M. Rao, E. Richter, S. Bandow, B. Chase, P.C. Eklund, K.A. Williams, S. Fang, K.R. Subbaswamy, M. Menon, A. Thess, R.E. Smalley, G. Dresselhaus, and M.S. Dresselhaus, Science **275**, 187 (1997).